Radical PolyMOFs: A Role for Ligand Dispersity in Enabling Crystallinity

Matthew A. Pearson, Mircea Dincă,* and Jeremiah A. Johnson*
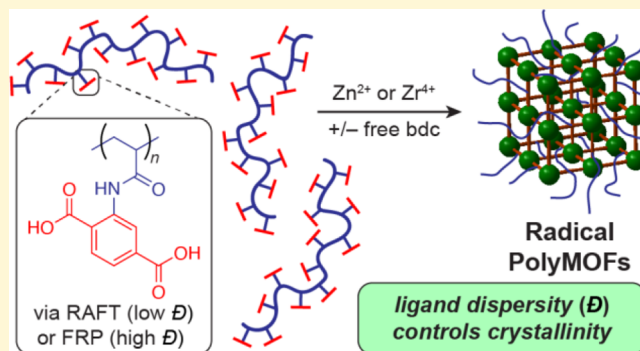
Read Online

ACCESS | Metrics & More | Article Recommendations | Supporting Information

ABSTRACT: Metal−organic frameworks (MOFs) derived from polymeric ligands ("polyMOFs") have been prepared from a limited set of polymerization methods. Herein, we report the synthesis of polyMOF ligands featuring MOF-forming benzenedicarboxylic acid (H_2bdc) linkers on their sidechains using common radical polymerization techniques: reversible addition fragmentation chain transfer (RAFT) polymerization and free radical polymerization (FRP). Interestingly, high-dispersity ligands prepared through FRP formed crystalline polyMOFs while low-dispersity ligands prepared through RAFT required the addition of free H_2bdc to yield crystalline materials analogous to MOF-5 (Zn) and UiO-66 (Zr). This work opens new opportunities for the development of next-generation polymer−MOF hybrids based on radical polymerization and suggests that ligand dispersity is a key design parameter for polyMOF synthesis.

INTRODUCTION

Metal−organic frameworks (MOFs) are a class of porous coordination polymer networks composed of metal clusters as junctions (referred to as secondary building units, SBUs) connected through organic linkers.[1] These materials have garnered extensive interest in recent years owing to their valuable properties, including high surface areas, open metal sites for catalysis, and modular syntheses,[2] which enable applications such as gas capture[3,4] and separation,[5,6] catalysis,[7−9] sensing,[10,11] and electronic devices.[12,13] Recently, efforts have focused on the development of hybrid materials comprising traditional amorphous or semicrystalline polymers and MOFs. Such hybrids could offer the processability and mechanical/chemical stability of traditional polymers without sacrificing the crystallinity and porosity of MOFs.[14−17]

One such class of hybrid materials, where MOF-forming organic linkers are covalently connected through a flexible macromolecular backbone, has been coined "polyMOFs."[18−20] Because the macromolecular ligands of polyMOFs contain organic linkers within their repeat units and are present during MOF crystallization, the polymer backbone can become integrated into the MOF lattice rather than, for example, coating the surface of preformed MOF crystals.[21,22] By mixing these macromolecular ligands with free ligands during MOF formation, it becomes possible to tune the amount of incorporated polymer and hence the final material properties, as has been demonstrated in the context of polyMOF nanoparticles.[23] More generally, polymer−MOF hybrids offer the potential to introduce a range of traditional synthetic polymer compositions into porous materials, providing

enhanced processability, tunability, and stability. Nevertheless, to the best of our knowledge, all the previously reported polyMOFs have utilized macromolecular ligands synthesized through either step-growth polymerizations,[18,24−27] multistep iterative exponential growth,[23,28] or under nonliving cationic polymerization conditions.[20]

Each of these examples has so far had key limitations, including poor control over ligand composition, molecular weight, and dispersity (Figure 1A) or access to only short (tetrameric) ligands (Figure 1B). Moreover, the only example of a chain-growth polymerization (cationic)[20] yielded materials with no permanent porosity. Meanwhile, radical polymerization, one of the most widely used polymerization methods, has not, to our knowledge, been used for polyMOF ligand synthesis. We reasoned that reversible deactivation radical polymerization (RDRP) processes could enable access to macromolecular ligands with higher molecular weights and narrow dispersities from new classes of monomers, opening opportunities to form polyMOFs with a wider variety of polymeric architectures and compositions (e.g., block copolymers) and allowing for a more detailed understanding of the roles of the ligand structure in defining polyMOF properties.
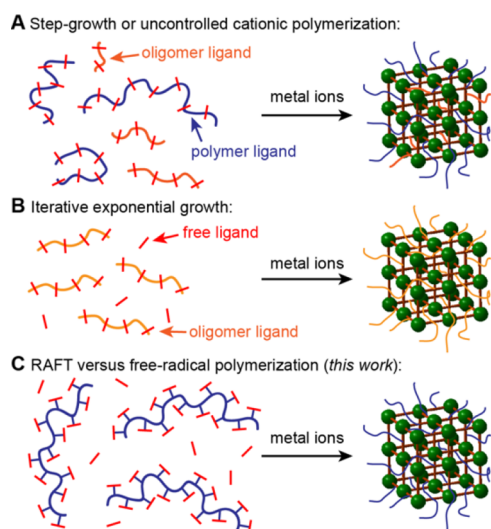
Figure 1. PolyMOFs have been formed from either (A) step-growth or cationic polymerizations that yield highly disperse mixtures (*Note*: the schematic depicts step-growth structures, with metal-coordinating sites embedded within the polymer backbone) or (B) iterative methods that provide discrete, yet short, ligands. Here (C), radical polymerizations—reversible addition fragmentation chain transfer (RAFT) and free radical polymerization (FRP)—are introduced to polyMOF synthesis. FRP is convenient yet it provides high-dispersity ligands. RAFT enables controlled ligand compositions with tunable molecular weights, low dispersities, and new compositions (acrylamides and block copolymers), but additional free ligands are required to form crystalline materials.

Herein, we report on the use of FRP as well as one of the most widely used RDRP methods—RAFT polymerization—for the synthesis of novel polyacrylamide-based macromolecular ligands bearing 1,4-bezenedicarboxylic acid (H_2bdc)-based sidechains.[29] RAFT-derived ligands, which feature low dispersities and tunable molecular weights, are combined with H_2bdc to form crystalline materials with tunable stabilities and Brunauer–Emmett–Teller (BET) surface areas. Moreover, the same ligands can be employed to generate two different classes of polyMOFs depending on the metal salt used, and they are amenable to chain extension to generate novel crystalline block-copolymer systems. Meanwhile, FRP-based ligands with high dispersity formed crystalline polyMOFs without addition of free H_2bdc, suggesting that ligand dispersity plays a key role in enabling polyMOF crystallization.

■ **EXPERIMENTAL SECTION**

Materials. Starting materials and solvents were purchased from commercial suppliers (Sigma-Aldrich, TCI, AK Scientific Inc.,

Cambridge Isotope Laboratories, Inc.). *N*-Isopropylacrylamide (NIPAM) was recrystallized from hexanes three times prior to use. Styrene was passed through a short basic alumina plug immediately prior to use. All other chemicals were used without purification.

Synthesis of PolyMOF Ligand by RAFT (pabdc-0a). Acrylamide monomer **abdc-0e** (200 mg, 0.76 mmol, 1 equiv), 2-(dodecylthiocarbonothioylthio)-2-methylpropionic acid (DDMAT) (8.3 mg, 0.022 mmol, 0.03 equiv), and azobisisobutyronitrile (AIBN) (1.3 mg, 0.0076 mmol, 0.01 equiv) were combined in a 3 mL dram vial. The vial was brought into a nitrogen-filled glovebox, where the solids were dissolved in anhydrous *N,N*-dimethylformamide (DMF) (2 mL). The solution was stirred and heated at 70 °C for 3 h. The reaction was quenched by submerging the vial into an ice bath and opening to air. The solvent was evaporated, and the remaining viscous yellow material was purified by preparatory gel permeation chromatography (Prep GPC) to give the isolated polymer as a powder. The trithiocarbonate end group was removed by stirring a solution of the polymer with lauroyl peroxide (4 equiv) and AIBN (40 equiv) in toluene at 70 °C overnight under nitrogen. The polymer was then isolated by Prep GPC. Hydrolysis was performed by addition of a 1 M aqueous solution of KOH (100 equiv) to a methanol solution of the polymer and stirring at 35 °C overnight. The product was precipitated with 1 M HCl.

**Synthesis of PolyMOF Ligand by FRP (pabdc-0a$_{conv}$).** Acrylamide monomer **abdc-0e** (100 mg, 0.38 mmol, 1 equiv) and AIBN (0.62 mg, 0.0038 mmol, 0.01 equiv) were combined in a 3 mL dram vial. In a nitrogen-filled glovebox, the solids were dissolved in anhydrous DMF (1 mL). The solution was then stirred at 70 °C overnight and then the reaction was quenched, and the solvent was evaporated. The crude solid was then dissolved in 10 mL of DMF, and a 1 M aqueous solution of KOH (3 mL) was added. The solution was stirred at 35 °C overnight, and the product was precipitated with 1 M HCl.

Representative Synthesis of Zn-Based PolyMOFs. In a 20 mL scintillation vial, 15 mg of **pabdc-0a**, the desired amount of 1,4-benzenedicarboxylic acid (H_2bdc), and 3 equiv of $Zn(NO_3)_2 \cdot 6H_2O$ (based on total H_2bdc, see the Supporting Information) were dissolved in 7 mL DMF. The vial was placed in a preheated isothermal oven at 100 °C for 24 h. A suspended white powder was collected by decanting the solution and centrifuging at 4000 rpm for 30 min. The powder was washed with anhydrous DMF (3 × 10 mL) by soaking for 30 min and isolation by centrifugation.

■ **RESULTS AND DISCUSSION**

The synthesis of polyMOF ligands with pendant metal-coordinating groups requires additional design parameters compared to step-growth methods wherein coordinating groups are embedded within the polymer backbone.[20] Two different dimensions can be tuned—the pendant sidechain length and the backbone spacer length. The former can be altered by changing the length of the linker between the coordinating group and the polymerizable functionality (here, an acrylamide). The average backbone distance could be tuned through statistical copolymerization with another monomer or

Scheme 1. Synthesis of Polyacrylamide Ligand pabdc-0a
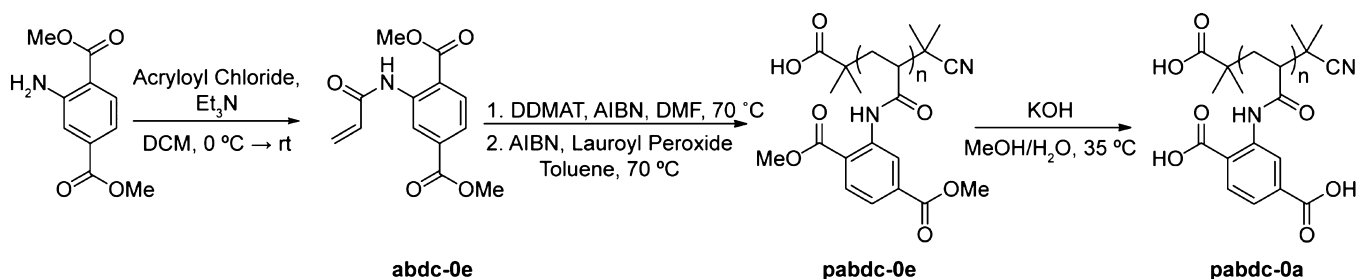
potentially through ring-opening polymerization of monomers varying in ring size. The copolymerization approach would enable facile access to a range of macromolecular ligands of various comonomer compositions and properties, as demonstrated below for block copolymers.

Here, we designed and synthesized two monomers—**abdc-3e** and **abdc-0e**—that feature three-carbon and zero-carbon spacers, respectively, between a polymerizable acrylamide and dimethyl bdc (Scheme 1, Figure S1). Monomer **abdc-3e** was prepared from 2-hydroxyterephthalic acid in four steps in 34.4% overall yield, while **abdc-0e** was prepared in one step from dimethyl aminoterephthalate and acryloyl chloride in 43.3% yield. To investigate their suitability for RAFT polymerization, each monomer was exposed to DDMAT and AIBN in DMF for 3−8 h at 70 °C under a N_2 atmosphere. The polymerizations displayed kinetic behavior indicative of RDRP processes (Figure S2).

Polymers of **abdc-3e** and **abdc-0e** had number-average molar masses of 6500 and 6400 g/mol, respectively, according to ^{1}H NMR and monomodal molar mass distributions with low dispersities ($Đ$ = 1.08 and 1.04, respectively) as determined by GPC (Figure S3, Table 1). ^{1}H NMR supported

**Table 1. Molar Mass and Dispersity of Polymer Ligands**

polymer ligand	$M_{n, GPC}$	$M_{n, NMR}$[a]	$Đ$
pabdc-0e	8360	6420	1.04
pabdc-0e$_{20k}$	21,640	20,089	1.18
pabdc-0e$_{conv}$	34,310		2.17
PSt-*b*-pabdc-0e	12,860	14,600	1.05
pabdc-3e	5380	6470	1.08
pabdc-3e-*co*-NIPAM 1:1	3480	4270	1.09
pabdc-3e-*co*-NIPAM 5:1	3970	4880	1.19

[a]Number-average molar masses were determined by end-group analysis using proton nuclear magnetic resonance (^{1}H NMR).

the proposed structures of the methyl ester polymers, showing the expected peak broadening and lack of monomer peaks (Figures S4 and S5). To demonstrate the utility of RAFT polymerization for the synthesis of polymer ligands of controlled length, a higher molar mass variant (M_n = 20,000 g/mol, $Đ$ = 1.18) of **abdc-0e** was also synthesized. The formation of statistical and block copolymers of **abdc-3e** and **abdc-0e** with NIPAM was also explored (*vide infra*, Figures S6 and S7).

To avoid any potential interference with MOF crystallization, the trithiocarbonate end groups of RAFT-derived polymers were removed by exposure to AIBN and lauroyl peroxide,[30] providing **pabdc-3e**, **pabdc-3e-*co*-NIPAM**, and **pabdc-0e** (Scheme 1, Figure S1). The number-average molar masses and dispersities were confirmed to be unchanged by this end-group removal process (Figure S8). Finally, saponification of the ester sidechains yielded the H_2bdc-functionalized ligands (e.g., **pabdc-0a**) as indicated by ^{1}H NMR spectroscopy (Figures 2, S9, and S10).

With these polymers in hand, we targeted the formation of polyMOF analogues of MOF-5, a well-known MOF composed of bdc linkers and Zn_4O-based SBUs. This MOF was chosen because of its relative ease of synthesis and as a point of comparison to polyMOFs of the same topology formed from step-growth polymer ligands reported by Cohen and co-workers.[18] Each polyacrylamide ligand was dissolved in DMF along with $Zn(NO_3)_2 \cdot 6H_2O$, and the mixtures were placed in a
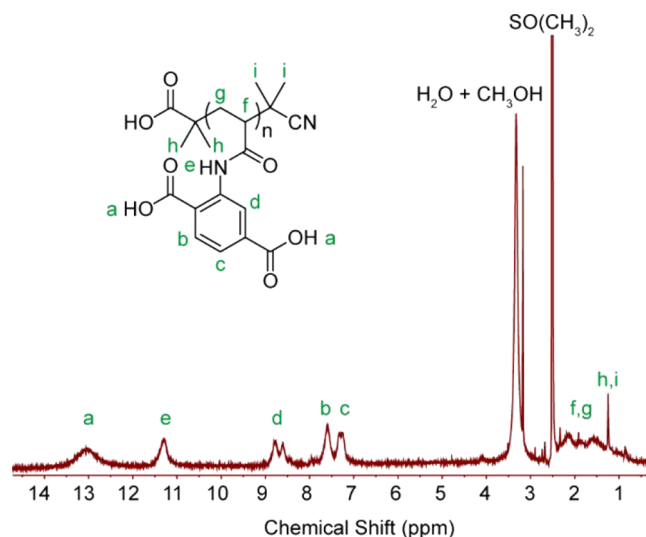

Figure 2. ^{1}H NMR (DMSO-d_6) spectrum of **pabdc-0a**.

preheated isothermal oven at 100 °C for 24 h.[31,32] Though similar conditions readily formed crystalline polyMOFs in Cohen's work, no crystalline materials were obtained using our RAFT-based ligands as determined by powder X-ray diffraction (PXRD). Moreover, the amorphous powder formed from **pabdc-0a** had a very low surface area (*vide infra*).

While the backbone and sidechain dimensions of our RAFT-based ligands may explain their inability to form crystalline polyMOFs, we hypothesized that their low dispersities may also play a key role, as low-dispersity ligands will have fewer oligomeric species that could fill gaps in the forming polyMOF lattice. This hypothesis was inspired by a report from Yazaki and co-workers,[20] which showed that high-dispersity polyvinyl ethers that have a similar backbone and sidechain spacings to our RAFT-based ligands could successfully generate crystalline polyMOFs. Additionally, Cohen and co-workers have shown that comparably lower dispersity polyether ligands form less crystalline or distorted crystalline structures compared to higher dispersity analogues.[26] To test our hypothesis, we synthesized a high-dispersity ($Đ$ = 2.17) variant of our polymer, **pabdc-0a$_{conv}$**, by FRP (Figures S11 and S12) and subjected this polymer to the same conditions used to form polyMOFs using the RAFT-based ligand **pabdc-0a**. Remarkably, this FRP-based ligand did indeed form crystalline polyMOFs with diffraction peaks matching MOF-5 (Figure S13). These results support the notion that increased dispersity facilitates polyMOF crystallization. Thus, to mimic this effect, we explored the addition of free H_2bdc to our low-dispersity RAFT-based polymer ligands. Compared to the use of disperse ligand mixtures, this approach offers a more controllable way to tune the polyMOF composition through rational mixing of high- and low-molecular-weight ligands. To our knowledge, this mixed ligand concept has not been applied to the formation of bulk polyMOFs or to systems using high-molecular-weight ligands.

Gratifyingly, upon addition of one, two, or three equivalents of H_2bdc per repeat unit of **pabdc-0a** to a solution of **pabdc-0a** and $Zn(NO_3)_2 \cdot 6H_2O$ (where the ratio of total H_2bdc, taken as the sum of H_2bdc units in **pabdc-0a** and free H_2bdc, to $Zn(NO_3)_2 \cdot 6H_2O$ was kept constant at 1:3), mixtures of white powders and visible crystals (the latter identified as MOF-5 by PXRD, Figure S14) were obtained. Separation of the white

powders (denoted as **Zn-pabdc-0a-1eq**, **Zn-pabdc-0a-2eq**, and **Zn-pabdc-0a-3eq**) was readily achieved by centrifugation at 200 rpm; following subsequent washing with DMF to remove any unbound ligands, PXRD of the isolated powders revealed lattice structures comparable to MOF-5 (Figure 3).

pabdc-0a + H_2bdc + $Zn(NO_3)_2 \cdot 6H_2O$ $\xrightarrow{\text{DMF, 100 °C}}$ **Zn-pabdc-0a-xeq**
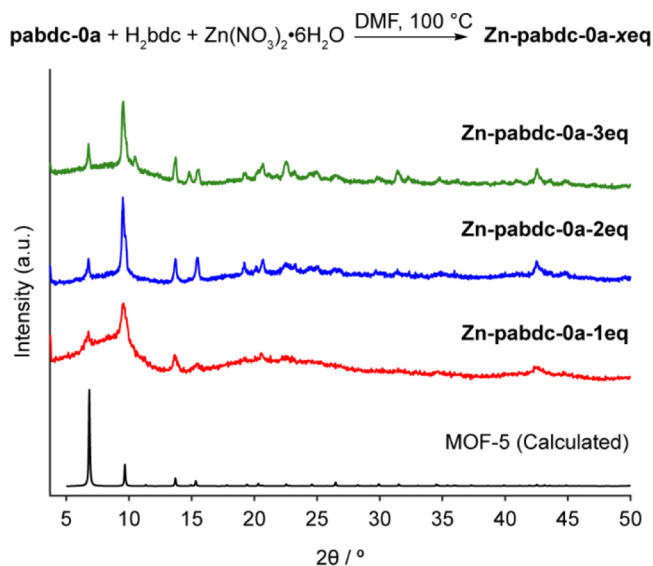
Figure 3. Powder X-ray diffractograms of **Zn-pabdc-0a-xeq**, polymer−MOF hybrids synthesized from **pabdc-0a**, and various equivalents of free H_2bdc.

Scanning electron microscopy (SEM) imaging of **Zn-pabdc-0a-2eq** (Figures 4, S15, and S16) revealed interconnected,
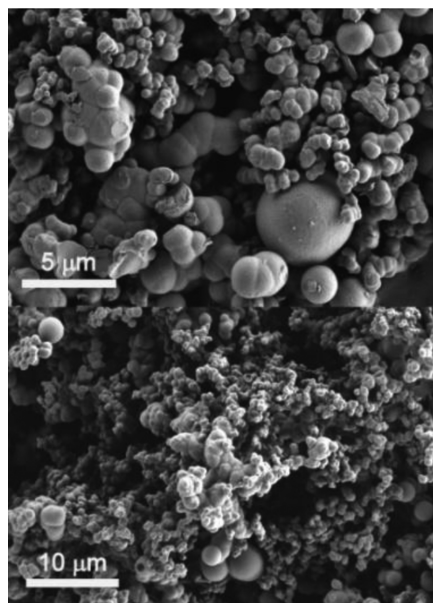

Figure 4. SEM images of **Zn-pabdc-0a-2eq**.

round particles with smooth surfaces, similar to reported polyMOFs and unlike the cubic crystals observed for MOF-5, mixtures of presynthesized MOF-5 and polymers, or polymer surface-coated MOF-5 crystals.[21] Fourier transform infrared spectroscopy (Figure S17) revealed that the carboxylate bands from the ligands were red-shifted, as expected upon coordination to Zn^{2+}.[33] Notably, high-molar mass **pabdc-**

$0a_{20k}$ (20 kDa) formed a comparable crystalline white powder under analogous conditions (Figure S18), showing that RAFT polymerization can be used to obtain polyMOF hybrid materials from polymer ligands with a range of molecular weights. By contrast, the addition of free H_2bdc to **pabdc-3a** or **pabdc-3a-co-NIPAM** produced a mixture of large, nonpolymer containing MOF-5 crystals (as determined by digestion and ^{1}H NMR) and an amorphous film (as determined by PXRD), suggesting that the pendant sidechain of this polymer ligand is too large to accommodate the 12 Å pore size and 8 Å aperture width of MOF-5, compared to the approximately 10.2 Å extended length of the pendant arm between the H_2bdc unit and the polymer backbone.[34,35]

Given that H_2bdc was added to form a crystalline powder with **pabdc-0a**, the question arises: is the polymer ligand truly incorporated into the MOF lattice, or is it simply coating the surface of separately formed MOF-5 crystals?[21,22] First, we note that we do not observe any obvious cubic MOF-5 crystals in the isolated powders by SEM imaging. Additionally, the fact that **pabdc-3a** does not form a crystalline powder suggests that surface binding is not the only operative mechanism, as a sidechain linker length should play less of a role in such cases. To further address this question, we digested **Zn-pabdc-0a-2eq** in $DCl/DMSO$-d_6 and quantified the ratio of free to polymer-bound H_2bdc by ^{1}H NMR analysis; the measured value, 1.66:1, matched the reaction stoichiometry of 2:1 well (Figure S19) especially considering that some visible MOF-5 crystals composed of H_2bdc were removed through centrifugation. Inductively coupled plasma-mass spectrometry showed that the powder contained 25.0% Zn by mass, slightly less than the 30.6% Zn that would be expected for the formula $Zn_4O(bdc)_{1.875}(pabdc)_{1.125}$ corresponding to the 1.66:1 ligand ratio, which could be a result of surface-bound polymer or polymer coordinated to Zn^{2+} ions not incorporated into the SBUs. Notably, however, if **pabdc-0a** was only bound to the surface of MOF-5 crystals of a typical size (2 μm), we would conservatively expect at least an order-of-magnitude greater ratio of free ligand to macromolecular ligand (see the Supporting Information for calculation). When the protected version of the polymer (**pabdc-0e**) was used with two equivalents of H_2bdc, visible crystallites matching MOF-5 by PXRD formed (Figure S20); they did not contain any polymer as determined from the ^{1}H NMR spectrum of the digested crystallites (Figure S21). This observation confirms that the crystalline powder could only be obtained when the polymer ligand is able to coordinate to the metal, as was also observed visually (Figure S22). Finally, MOF-5 crystals were presynthesized and placed in a solution of **pabdc-0a** in DMF at 100 °C for 24 h, following similar conditions to those used in the literature to attach polymers to the surface of MOF-5 crystals.[21] PXRD analysis of the materials isolated after this treatment no longer matched the patterns of MOF-5 (Figures S23 and S24), showing that **pabdc-0a** is not capable of coordinating to the surfaces of presynthesized MOF-5 crystals to form stable MOF-5 analogues under these conditions. Instead, degradation of the MOF-5 structure is observed. Altogether, these observations strongly suggest that **pabdc-0a** is integrated into the lattice of these materials; however, we note that our results cannot rule out the presence of some small (<150 nm) MOF-5 particles mixed with polymer.

Encouraged by these results, we further investigated the impact of the number of equivalents of free H_2bdc on the crystallinity and stability of these materials. Comparing the

PXRD patterns (Figure 3), broader peaks are observed when only one equivalent of free H_2bdc is used, suggesting lower crystallinity. We hypothesized that samples formed in the presence of more H_2bdc would display properties like the native MOF-5 while those made from fewer equivalents may display properties more reflective of their polymeric ligand, offering a versatile way to tune the properties of these hybrid materials. This hypothesis was supported by time-dependent stability studies under an ambient atmosphere (Figures 5 and
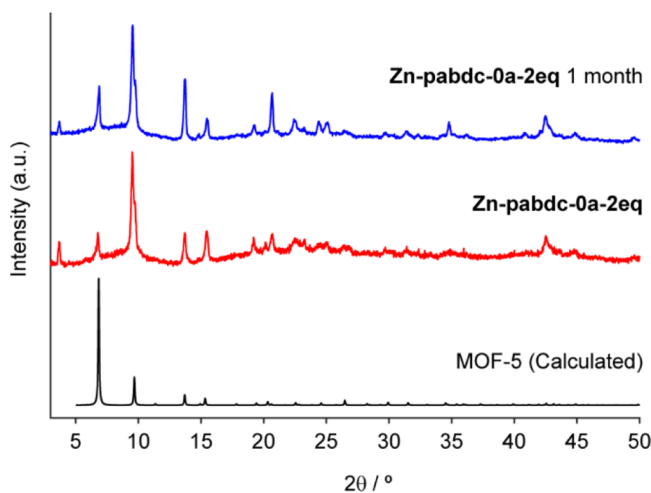
Figure 5. Powder X-ray diffractograms of **Zn-pabdc-0a-2eq** as-synthesized and after being stored under ambient conditions for 1 month.

S25−S27). MOF-5 is known to be unstable under ambient conditions because of the lability of the Zn−O bonds.[36] Isoreticular polyMOFs, by contrast, can exhibit improved hydrolytic stability.[27,26] Notably, while **Zn-pabdc-0a-3eq** decomposed after 2 months under ambient conditions, based on the disappearance of the PXRD peak at 6.8°, both **Zn-pabdc-0a-2eq** and **Zn-pabdc-0a-1eq** retained their PXRD patterns, implying that they had maintained their crystallinity.

The permanent porosities of **Zn-pabdc-0a-1eq**, **Zn-pabdc-0a-2eq**, and **Zn-pabdc-0a-3eq** as well as the amorphous powder **Zn-pabdc-0a** were probed with N_2 gas sorption measurements. Type-I isotherms were observed, indicating microporosity, with calculated BET surface areas of 11, 47, 92, and 138 m^2/g for **Zn-pabdc-0a**, **Zn-pabdc-0a-1eq**, **Zn-pabdc-0a-2eq**, and **Zn-pabdc-0a-3eq**, respectively (Figure S28). The BET surface areas of these hybrid materials are lower than those reported for many isoreticular polyMOFs formed through step-growth polymerization methods or polymer-coated MOF crystals (~200 to 1100 m^2/g), which is likely the result of greater pore-filling from the polymer chains as a consequence of the sidechain versus main-chain ligand location (Figure 1).[18,24,28] Regardless, these results suggest that RAFT-based ligands can be used to generate polyMOF hybrid materials with accessible permanent porosity and that the accessible volume can be rationally tuned via the polymer/spacer ligand reaction stoichiometry. In the future, it will be interesting to further optimize the radical polyMOF monomers to optimize material surface areas and other key properties.

Next, the generality of our approach was investigated through the synthesis of UiO-66 analogues. Once again, in the absence of H_2bdc, only an amorphous powder was observed upon subjecting **pabdc-0a** to typical UiO-66

synthesis conditions. Addition of one, two, or three equivalents of free H_2bdc per polymer repeat unit, however, yielded crystalline white powders with PXRD reflections matching those of UiO-66 (Figure S29).[37] Digestion of these powders in D_2SO_4/DMSO-d_6 and subsequent ^{1}H NMR analysis confirmed the incorporation of **pabdc-0a**, with ratios of free to polymer-bound H_2bdc matching the initial reaction stoichiometry (Figure S30). Comparison of **Zr-pabdc-0a-2eq** synthesized both with and without formic acid as a modulator showed that exclusion of the formic acid led to narrower peak widths in the PXRD diffractogram (Figure S31) and an increase in the ratio of free to polymer-bound H_2bdc in the digested sample from 2.2 to 3.2 (Figure S32), suggesting that the slowed kinetics imposed by the modulator aids the incorporation of the polymer ligand.

Because of its controlled nature and excellent end-group fidelity, RAFT polymerization is a powerful tool for block-copolymer synthesis. To explore the potential for the formation of diblock copolymers featuring a polyMOF-forming domain, a novel block-copolymer ligand—**PSt-*b*-pabdc-0a**—was synthesized through the sequential polymerizations of styrene and **abdc-0a** (Figures 6a and S33). **PSt-*b*-pabdc-0a**
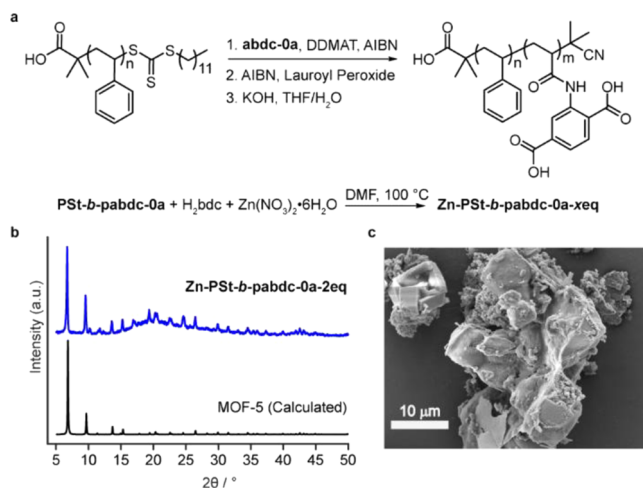
Figure 6. Synthesis of macromolecular ligand **PSt-*b*-pabdc-0a** (a) and powder X-ray diffractogram (b) and SEM images (c) of **Zn-PSt-*b*-pabdc-0a-2eq** formed from the ligand and two equivalents of H_2bdc.

was subjected to the same conditions used to synthesize **Zn-pabdc-0a-2eq** above. Interestingly, while no precipitate was apparent after 24 h at 100 °C, a flaky white precipitate formed after an additional 24 h. The PXRD pattern of this solid matched that of MOF-5 (Figure 6b), and digestion of the powder confirmed that it contains the polymer ligand (Figure S34). The material consisted of interconnected cubic particles with rounded edges as determined by SEM (Figure 6c), which is notably different from the spherical morphology observed for the homopolymer ligands above. This result suggests that the presence of the polystyrene block may lead to preferential binding of the macromolecular ligand to the surface of MOF crystals, leading to phase-separated structures.

■ CONCLUSIONS

Here, we describe a new strategy for polyMOF hybrid material synthesis using polymer ligands synthesized by radical polymerization (specifically, RAFT and FRP). RAFT offers improved control over the composition, molar mass, and

dispersity of the polymer ligands used for polyMOF synthesis and offers a simple way to rationally tune material properties. Moreover, RAFT facilitates block-copolymer synthesis, allowing for further expansion of the scope of these materials. In the future, this approach will allow for the exploration of multiblock ligands and the synthesis of complex ligand architectures such as star and graft copolymers. Finally, this work provides evidence that polymer ligand dispersity plays a key role in polyMOF formation: more heterogeneous polymer ligands (i.e., higher dispersity) lead to more crystalline materials. This observation should further spur interest in tuning polymer dispersity, either through advanced polymerization methods or mixing of ligands of different sizes, to further optimize the properties of polymer–MOF hybrid materials.

■ ASSOCIATED CONTENT

Ⓢ Supporting Information

The Supporting Information is available free of charge at https://pubs.acs.org/doi/10.1021/acs.chemmater.1c02411.

> Experimental procedures, synthetic procedures, ^{1}H NMR spectra, kinetics data, GPC data, UV−vis spectra, PXRD data, thermogravimetry analysis data, and SEM data (PDF)

■ AUTHOR INFORMATION

Corresponding Authors

Mircea Dincă − *Department of Chemistry, Massachusetts Institute of Technology, Cambridge, Massachusetts 02139, United States;* ⓞ orcid.org/0000-0002-1262-1264; Email: mdinca@mit.edu

Jeremiah A. Johnson − *Department of Chemistry, Massachusetts Institute of Technology, Cambridge, Massachusetts 02139, United States;* ⓞ orcid.org/0000-0001-9157-6491; Email: jaj2109@mit.edu

Author

Matthew A. Pearson − *Department of Chemistry, Massachusetts Institute of Technology, Cambridge, Massachusetts 02139, United States*

Complete contact information is available at:
https://pubs.acs.org/10.1021/acs.chemmater.1c02411

Notes

The authors declare no competing financial interest.
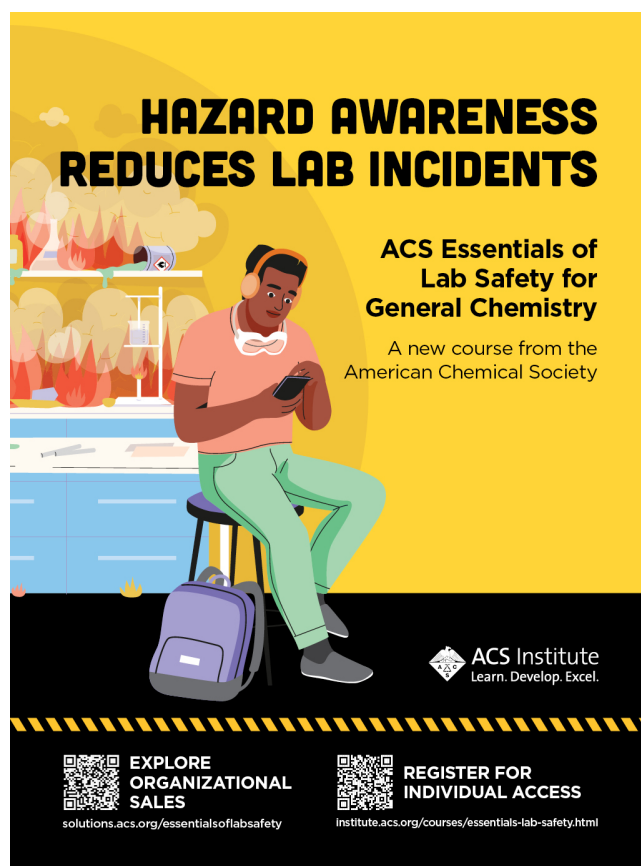
■ ACKNOWLEDGMENTS

■ REFERENCES

(1) Furukawa, H.; Cordova, K. E.; O'keeffe, M.; Yaghi, O. M. The Chemistry and Applications of Metal-Organic Frameworks. *Science* **2013**, *341*, 974.

(2) Czaja, A. U.; Trukhan, N.; Müller, U. Industrial Applications of Metal-Organic Frameworks. *Chem. Soc. Rev.* **2009**, *38*, 1284−1293.

(3) Mason, J. A.; Veenstra, M.; Long, J. R. Evaluating Metal-Organic Frameworks for Natural Gas Storage. *Chem. Sci.* **2014**, *5*, 32−51.

(4) Murray, L. J.; Dincă, M.; Long, J. R. Hydrogen Storage in Metal-Organic Frameworks. *Chem. Soc. Rev.* **2009**, *38*, 1294−1314.

(5) Adil, K.; Belmabkhout, Y.; Pillai, R. S.; Cadiau, A.; Bhatt, P. M.; Assen, A. H.; Maurin, G.; Eddaoudi, M. Gas/Vapour Separation Using Ultra-Microporous Metal-Organic Frameworks: Insights into the Structure/Separation Relationship. *Chem. Soc. Rev. R. Soc. Chem.* **2017**, *46*, 3402−3430.

(6) Li, J.-R.; Sculley, J.; Zhou, H.-C. Metal−Organic Frameworks for Separations. *Chem. Rev.* **2012**, *112*, 869−932.

(7) Lee, J.; Farha, O. K.; Roberts, J.; Scheidt, K. A.; Nguyen, S. T.; Hupp, J. T. Metal-Organic Framework Materials as Catalysts. *Chem. Soc. Rev.* **2009**, *38*, 1450−1459.

(8) Jiao, L.; Wang, Y.; Jiang, H.-L.; Xu, Q. Metal-Organic Frameworks as Platforms for Catalytic Applications. *Adv. Mater.* **2018**, *30*, No. 1703663.

(9) Yang, D.; Gates, B. C. Catalysis by Metal Organic Frameworks: Perspective and Suggestions for Future Research. *ACS Catal.* **2019**, *9*, 1779−1798.

(10) Kumar, P.; Deep, A.; Kim, K. H. Metal organic frameworks for sensing applications. *Trends Analyt. Chem.* **2015**, *73*, 39−53.

(11) Stassen, I.; Dou, J.-H.; Hendon, C.; Dincă, M. Chemiresistive Sensing of Ambient CO_2 by an Autogenously Hydrated Cu_3 (Hexaiminobenzene)$_2$ Framework. *ACS Cent. Sci.* **2019**, *5*, 1425−1431.

(12) Sun, L.; Campbell, M. G.; Dincă, M. Electrically Conductive Porous Metal-Organic Frameworks. *Angew. Chem. Int. Ed.* **2016**, *55*, 3566−3579.

(13) Hendon, C. H.; Rieth, A. J.; Korzyński, M. D.; Dincă, M. Grand Challenges and Future Opportunities for Metal−Organic Frameworks. *ACS Cent. Sci.* **2017**, *3*, 554−563.

(14) Kitao, T.; Zhang, Y.; Kitagawa, S.; Wang, B.; Uemura, T. Hybridization of MOFs and Polymers. *Chem. Soc. Rev. R. Soc. Chem.* **2017**, *46*, 3108−3133.

(15) Gu, Y.; Zhao, J.; Johnson, J. A. Polymer Networks: From Plastics and Gels to Porous Frameworks. *Angew. Chem. Int. Ed.* **2020**, *59*, 5022−5049.

(16) Kalaj, M.; Bentz, K. C.; Ayala, S.; Palomba, J. M.; Barcus, K. S.; Katayama, Y.; Cohen, S. M. MOF-Polymer Hybrid Materials: From Simple Composites to Tailored Architectures. *Chem. Rev.* **2020**, *120*, 8267−8302.

(17) Pastore, V. J.; Cook, T. R. Coordination-Driven Self-Assembly in Polymer−Inorganic Hybrid Materials. *Chem. Mater.* **2020**, *32*, 3680−3700.

(18) Zhang, Z.; Nguyen, H. T. H.; Miller, S. A.; Cohen, S. M. PolyMOFs: A Class of Interconvertible Polymer-Metal-Organic-Framework Hybrid Materials. *Angew. Chem. Int. Ed.* **2015**, *54*, 6152−6157.

(19) Ayala, S.; Bentz, K. C.; Cohen, S. M. Block Co-PolyMOFs: Morphology Control of Polymer-MOF Hybrid Materials. *Chem. Sci.* **2019**, *10*, 1746−1753.

(20) Yazaki, K.; Takahashi, M.; Miyajima, N.; Obata, M. Construction of a PolyMOF Using a Polymer Ligand Bearing the Benzenedicarboxylic Acid Moiety in the Side Chain. *New J. Chem.* **2020**, *44*, 5182−5185.

(21) Pastore, V. J.; Cook, T. R.; Rzayev, J. Polymer−MOF Hybrid Composites with High Porosity and Stability through Surface-Selective Ligand Exchange. *Chem. Mater.* **2018**, *30*, 8639−8649.

(22) Barcus, K.; Cohen, S. M. Free-Standing Metal-Organic Framework (MOF) Monolayers by Self-Assembly of Polymer-Grafted Nanoparticles. *Chem. Sci.* **2020**, *11*, 8433−8437.

(23) Gu, Y.; Huang, M.; Zhang, W.; Pearson, M. A.; Johnson, J. A. PolyMOF Nanoparticles: Dual Roles of a Multivalent PolyMOF Ligand in Size Control and Surface Functionalization. *Angew. Chem. Int. Ed.* **2019**, *58*, 16676−16681.

(24) Palomba, J. M.; Ayala, S.; Cohen, S. M. PolyMOF Formation from Kinked Polymer Ligands via *Ortho*-Substitution. *Isr. J. Chem.* **2018**, *58*, 1123−1126.

(25) Schukraft, G. E. M.; Ayala, S.; Dick, B. L.; Cohen, S. M. Isoreticular Expansion of PolyMOFs Achieves High Surface Area Materials. *Chem. Commun.* **2017**, *53*, 10684−10687.

(26) Ayala, S.; Zhang, Z.; Cohen, S. M. Hierarchical Structure and Porosity in UiO-66 PolyMOFs. *Chem. Commun.* **2017**, *53*, 3058−3061.

(27) Zhang, Z.; Nguyen, H. T. H.; Miller, S. A.; Ploskonka, A. M.; Decoste, J. B.; Cohen, S. M. Polymer-Metal-Organic Frameworks (PolyMOFs) as Water Tolerant Materials for Selective Carbon Dioxide Separations. *J. Am. Chem. Soc.* **2016**, *138*, 920−925.

(28) Macleod, M. J.; Johnson, J. A. Block Co-PolyMOFs: Assembly of Polymer-PolyMOF Hybrids: Via Iterative Exponential Growth and "Click" Chemistry. *Polym. Chem.* **2017**, *8*, 4488−4493.

(29) Perrier, S. 50th Anniversary Perspective: RAFT Polymerization - A User Guide. *Macromolecules* **2017**, *50*, 7433−7447.

(30) Chen, M.; Moad, G.; Rizzardo, E. Thiocarbonylthio End Group Removal from RAFT-Synthesized Polymers by a Radical-Induced Process. *J. Polym. Sci. A Polym. Chem.* **2009**, *47*, 6704−6714.

(31) Eddaoudi, M.; Kim, J.; Rosi, N.; Vodak, D.; Wachter, J.; O'Keeffe, M.; Yaghi, O. M. Systematic Design of Pore Size and Functionality in Isoreticular MOFs and Their Application in Methane Storage. *Science* **2002**, *295*, 469−472.

(32) Kaye, S. S.; Dailly, A.; Yaghi, O. M.; Long, J. R. Impact of Preparation and Handling on the Hydrogen Storage Properties of Zn4O(1,4-Benzenedicarboxylate)3 (MOF-5). *J. Am. Chem. Soc.* **2007**, *129*, 14176−14177.

(33) Zhang, Z.; Chen, Y.; Xu, X.; Zhang, J.; Xiang, G.; He, W.; Wang, X. Well-Defined Metal-Organic Framework Hollow Nanocages. *Angew. Chem. Int. Ed.* **2014**, *53*, 429−433.

(34) Tsao, C. S.; Yu, M. S.; Chung, T. Y.; Wu, H. C.; Wang, C. Y.; Chang, K.; Chen, H. L. Characterization of Pore Structure in Metal-Organic Framework by Small-Angle X-Ray Scattering. *J. Am. Chem. Soc.* **2007**, *129*, 15997−16004.

(35) Pyykkö, P.; Atsumi, M. Molecular Double-Bond Covalent Radii for Elements Li-E112. *Chem. - A Eur. J.* **2009**, *15*, 12770−12779.

(36) Rieth, A. J.; Wright, A. M.; Dincă, M. Kinetic Stability of Metal−Organic Frameworks for Corrosive and Coordinating Gas Capture. *Nat. Rev. Mater.* **2019**, *4*, 708−725.

(37) Schaate, A.; Roy, P.; Godt, A.; Lippke, J.; Waltz, F.; Wiebcke, M.; Behrens, P. Modulated Synthesis of Zr-Based Metal-Organic Frameworks: From Nano to Single Crystals. *Chem. - A Eur. J.* **2011**, *17*, 6643−6651.